PAPER

Construction of efficient blue AIE emitters with triphenylamine and TPE moieties for non-doped OLEDs†

Jing Huang,[a] Yibin Jiang,[b] Jie Yang,[a] Runli Tang,[a] Ni Xie,[c] Qianqian Li,[a] Hoi Sing Kwok,[b] Ben Zhong Tang[c] and Zhen Li*[a]

In this paper, by merging the hole-dominated triphenylamine (**TPA**) and tetraphenylethene (**TPE**) moieties together with different linkage positions, four derivatives of 1,2-bis[4′-(diphenylamino)biphenyl-4-yl]-1,2-diphenylethene (**2TPATPE**) were successfully synthesized with confirmed structures, and their thermal, optical and electronic properties were fully investigated. Thanks to the introduction of the *meta*-linkage mode on the **TPE** core, their π-conjugation length could be effectively restricted to ensure blue emission. The non-doped OLEDs based on these four emitters exhibit blue emissions from 443–466 nm, largely blue-shifted with respect to the green emission of **2TPATPE** (514 nm). Meanwhile, good electroluminescence efficiencies with L_{max}, $\eta_{C,max}$, and $\eta_{P,max}$ of up to 8160 cd m^{-2}, 3.79 cd A^{-1}, and 2.94 lm W^{-1} respectively, have also been obtained, further validating our rational design of blue AIE fluorophores.

Introduction

Organic light-emitting diodes (OLEDs) have attracted considerable attention owing to their promising applications in flat-panel displays and solid-state lighting resources.[1] In order to obtain full-color OLEDs, the hunt for highly efficient and stable blue emitters has become a pressing issue.[2] Because of the wide-band-gap nature of blue emitters, their electroluminescence (EL) performance is often inferior to those of the other two primary-color (red and green) emitters.[3] Moreover, most conventional fluorophores suffer badly from the notorious aggregation-caused quenching (ACQ) effect when fabricated as thin solid films in the devices.[4] Although various chemical and physical approaches have been utilized to alleviate the ACQ effect, such as the attachment of bulky alicyclics and using guest–host doped emitter systems, they have met with limited success and there are also sometimes side effects, as the formation of aggregates is an intrinsic process when fluorophores are located in close vicinity to one another.[5] To solve

this problem as simply as possible, the use of molecules with distinctive luminogenic characteristics, *i.e.* taking advantage of molecular aggregation, might be a viable solution.

In 2001, Ben Zhong Tang's group observed an intriguing phenomenon termed 'aggregation-induced emission' (AIE), which is exactly the opposite of the ACQ effect: a series of propeller-like molecules are nearly non-emissive in solution but emit intensely in the aggregated state.[6] They have also rationalized the restriction of intramolecular rotation (RIR) as the main cause for the AIE effect based on their systematic research.[7] Consequently, this unique luminogenic characteristic renders AIE-active molecules promising candidates for OLEDs. Among the reported AIE fluorophores, tetraphenylethene (**TPE**) is an iconic molecule owing to its facile synthesis and splendid AIE effect.[8] But **TPE** itself is not a good emitter although its EL emission is in the deep-blue region. Recently, by directly attaching **TPE** to some classical ACQ chromophores, new AIE emitters with outstanding EL performance have been generated.[9] However, few blue AIE luminogens have been reported, because it is difficult to retain both the good EL performance and large band gaps of the molecules. For example, by just linking two **TPE** blocks together through the *para* linkage mode, the resultant 4,4′-bis(1,2,2-triphenylvinyl)biphenyl (**BTPE**) exhibits an electroluminescence (EL) performance with a current efficiency of up to 7.3 cd A^{-1},[9c] much higher than that of **TPE** (0.45 cd A^{-1}). But the EL emission is red-shifted from deep blue to sky blue (445 to 488 nm), as a result of the good conjugation effect between the two **TPE** moieties (Chart 1).

Recently, in an attempt to overcome this problem, we have reported an efficient approach of using different linkage modes

[a]*Department of Chemistry, Hubei Key Lab on Organic and Polymeric Opto-Electronic Materials, Wuhan University, Wuhan 430072, China. E-mail: lizhen@whu.edu.cn; lichemlab@163.com; Fax: +86-27-68755363; Tel: +86-27-68755363*

[b]*Department of Electronic and Computer Engineering, The Hong Kong University of Science & Technology, Clear Water Bay, Kowloon, Hong Kong, China*

[c]*Department of Chemistry, The Hong Kong University of Science & Technology, Clear Water Bay, Kowloon, Hong Kong, China*

† Electronic supplementary information (ESI) available: Chemical structures of **BTPE** and its derivatives, AIE curves, optimized molecular structures and CV plots for *p***TPE**-2*m***TPA**, *m***TPE**-2*o***TPA**, *m***TPE**-2*m***TPA** and *m***TPE**-2*p***TPA**. See DOI: 10.1039/c3tc32207f

2028 | *J. Mater. Chem. C*, 2014, **2**, 2028–2036
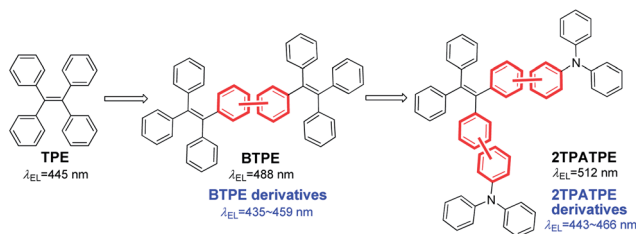
This journal is © The Royal Society of Chemistry 2014

Chart 1 Schematic structures and maximum EL emissions of TPE, BTPE, 2TPATPE and their derivatives.

to construct blue or deep-blue AIE emitters.[10] As the first example, a series of **BTPE** derivatives (Chart S1†), simply constructed from two **TPE** groups with *ortho-*, *meta-* or *para-*linkage modes, have been successfully synthesized.[10c] The device data demonstrate that all the molecules exhibit deep-blue emissions ranging from 435 to 459 nm, with good electroluminescence efficiencies of up to 2.8 cd A^{-1}. Apparently, the π-conjugation lengths of the four derivatives were effectively shortened by using different linking positions of the two **TPE** units. In addition, we have also found that it is more effective to attach **TPE** to other chromophores through its *meta-*positions for both reducing intramolecular conjugation and retaining good EL performance. Is this a general rule for the design of blue or deep-blue AIE luminogens, or only special case for the **BTPE** system? With this question in mind, we tried to apply the *meta* linkage mode to some other AIE luminogens. **2TPATPE** (Chart 2), constructed from hole-dominated triphenylamine (**TPA**) and **TPE** units through the *para* linkage mode, exhibited good hole-transporting ability and outstanding improvement in EL performance with a current efficiency of up to 13.0 cd A^{-1} (*cf.* 0.45 cd A^{-1} for **TPE**).[9g] Nevertheless, its EL emission is largely red-shifted to 514 nm (*cf.* 445 nm for **TPE**), due to the good conjugation between the **TPA** and **TPE** units. In addition, owing to the synthetic method employed for **2TPATPE**, it is a mixture of *E*- and *Z*-isomers, which may influence the molecular array in the thin solid films and the charge transfer of the
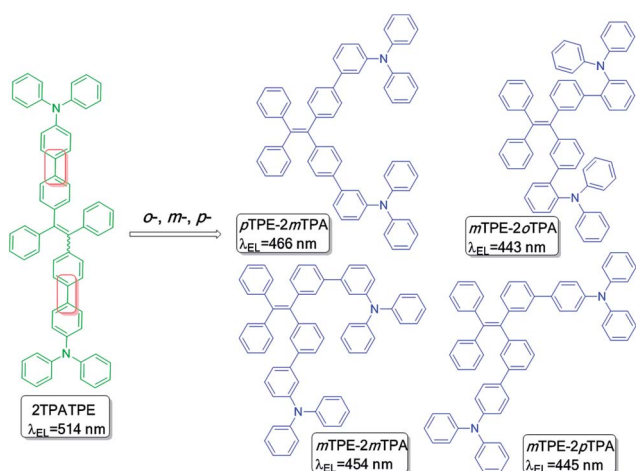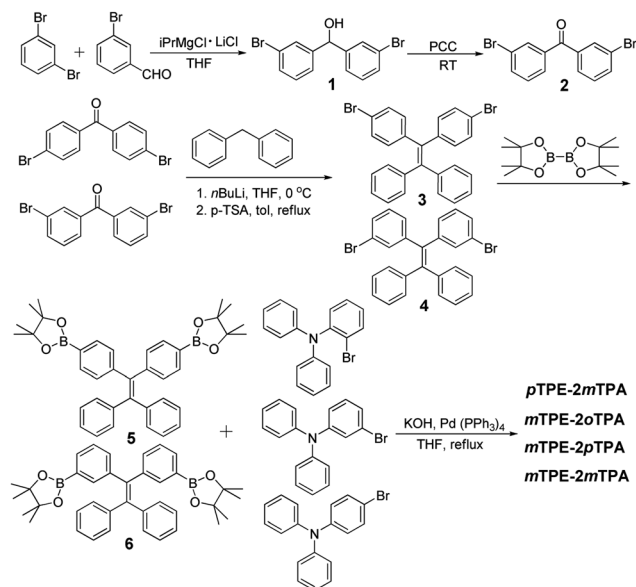
devices. Then, is it possible to generate blue fluorophores through the minor and facile structural modification? Perhaps, the *meta* linkage mode could realize this point.

Consequently, in this work, we have synthesized four **2TPATPE** derivatives to further confirm our idea of generating blue or deep-blue AIE emitters by changing the linkage modes. As shown in Chart 2, all the four compounds possess definite chemical structures without any isomers. First, we have undertaken a facile synthesis to obtain *p***TPE**-2*m***TPA**. Compared to **2TPATPE** (514 nm), its EL emission is largely blue-shifted to 466 nm. Inspired by this exciting result, three other **2TPATPE** derivatives, *m***TPE**-2*o***TPA**, *m***TPE**-2*m***TPA** and *m***TPE**-2*p***TPA**, have also been synthesized, by attaching **TPA** moieties to the **TPE** core through our favorite *meta* linkage mode. As a result, the large band gaps resulting from the less conjugated linkage mode are retained to ensure their emissions are still located in the blue region. Gratifyingly, the device performances are consistent with our expectations: when fabricated as emissive layers in non-doped OLEDs, all these three emitters exhibit blue emissions ranging from 443 to 454 nm, with Commission Internationale de l'Eclairage (CIE) chromaticity coordinates of (0.16, 0.13), (0.16, 0.16) and (0.16, 0.15). Although the device configurations have not yet been optimized, the highest L_{max} is up to 3.79 cd A^{-1}, which is much higher than that of **TPE** (0.45 cd A^{-1}), showing the superiority of this minor structural modification. Herein, we would like to present the synthesis, photophysical properties, theoretical calculations and electroluminescence of the four **2TPATPE** derivatives in detail.

Results and discussion

Synthesis

Scheme 1 illustrates the synthetic routes to *p***TPE**-2*m***TPA**, *m***TPE**-2*o***TPA**, *m***TPE**-2*m***TPA** and *m***TPE**-2*p***TPA**, and the detailed

Chart 2 Chemical structures of TPE-2TPA reported previously and its derivatives investigated in this work.

Scheme 1 Synthetic routes to *p*TPE-2*m*TPA, *m*TPE-2*o*TPA, *m*TPE-2*p*TPA, and *m*TPE-2*m*TPA.

This journal is © The Royal Society of Chemistry 2014

J. Mater. Chem. C, 2014, **2**, 2028–2036 | **2029**

procedures are presented in the experimental section. As the key intermediate, 3,3′-dibromobenzophenone, was synthesized from 1,3-dibromobenzene and 3-bromobenzaldehyde through the PCC (pyridinium chlorochromate) oxidation reaction in two steps.[11] Then 4,4′-dibromobenzophenone and the obtained compound **2** were reacted with diphenylmethane to yield dibromo-**TPE** **3** and **4** without isomers, showing some advantages over the MucMurry reaction employed for the synthesis of **2TPATPE**. The corresponding **TPE** diboronic esters **5** and **6** were successfully synthesized in good yields using Pd(dppf)$_2$Cl$_2$ as the catalyst. Moreover, 2-bromotriphenyamine, 3-bromo-triphenylamine and 4-bromotriphenylamine were obtained according to procedures from the literature.[13] Finally, the desired products were successfully obtained through the Suzuki cross-coupling reactions of **TPE** diboronic esters **5–6** with bro-motriphenylamine, in the presence of a catalytic amount of Pd(PPh$_3$)$_4$, in 2M KOH aqueous solution, and a THF/H$_2$O 3 : 1 mixed solution. All the products were purified by column chromatography through a silica gel stationary phase using petroleum ether and dichloromethane as eluent, and fully characterized by ^{1}H and ^{13}C NMR, mass spectrometry, and elemental analysis.

Thermal properties

The thermal properties of the four **2TPATPE** derivatives were characterized by thermal gravimetric analyses (TGA, Fig. 1) and differential scanning calorimetry (DSC) under an atmosphere of nitrogen, and the corresponding data is summarized in Table 1. All of the four compounds exhibit high thermal decomposition temperatures (T_d, corresponding to 5% weight loss) ranging from 411–457 °C. Among them, *m*TPE-2*o*TPA possesses the lowest T_d value, probably due to its highly twisted conformation. We have only observed the glass transition temperatures (T_g) for *m*TPE-2*m*TPA and *m*TPE-2*p*TPA with T_g values of 82 and 87 °C, which are higher than that of the common blue fluorescent material 4,4′-bis(2,2′-diphenyl vinyl)-1,1′-biphenyl (DPVBi, 64 °C).[12] The good thermal stability with high T_d and T_g values will be beneficial to the preparation of homogenous and

amorphous thin films during the vaccum-deposition process, ensuring the subsequent operating stability and good EL performance of the resulting devices.

Optical properties

All of the four **2TPATPE** derivatives are soluble in common organic solvents, such as tetrahydrofuran (THF), toluene, dichloromethane and chloroform, but insoluble in water. Fig. 2 shows the UV-vis absorption spectra of the four luminogens in dilute THF (∼1 μM). The maximum absorption wavelengths ($\lambda_{abs,max}$) of *p*TPE-2*m*TPA, *m*TPE-2*o*TPA, *m*TPE-2*m*TPA and *m*TPE-2*p*TPA are 350, 300, 299 and 327 nm, respectively, which are more blue-shifted, by as much as 61 nm, than that of **2TPATPE** (360 nm), partially confirming the efficient approach for conjugation adjustment by simply conveniently changing the linkage modes. For *m*TPE-2*o*TPA and *m*TPE-2*m*TPA, their maximum absorptions are almost identical to that of **TPE** (299 nm), showing their limited intramolecular conjugation despite of the presence of two extra **TPA** units. *m*TPE-2*p*TPA has the largest maximum absorption wavelength (327 nm), showing its longer conjugation length. This could be explained by its more planar optimized structure (Fig. S2†). While *m*TPE-2*o*TPA has a much shorter conjugation length resulting from it having the most twisted conformation. Importantly, in comparison with *p*TPE-2*m*TPA, *m*TPE-2*m*TPA is less-conjugated upon the introduction of the two *meta*-linked **TPA** groups to the **TPE** core, shedding some light on the further construction of deep-blue emitters by using the *meta*-**TPE** building blocks.

In order to study the AIE characteristic of the four **2TPATPE** derivatives, we chose water and THF as the solvent pair for their miscibility, to investigate the photoluminescence (PL) properties of the obtained **2TPATPE** derivatives. Fig. S1† shows the PL spectra of the new fluorophores in THF/water mixtures with different water fractions (f_w), which enabled fine-tuning of the solvent polarity and the extent of solute aggregation. It can be clearly seen that, when molecules were readily dissolved in pure THF solutions, the PL curves are all practically a flat line parallel to the abscissa, showing their faint emission property in the solution state. With the gradual addition of water, the PL intensities of the four compounds remain low in aqueous mixtures with a water content less than 60%, above which, they increase swiftly with clear peaks becoming apparent in the emission spectra. At a f_w value of 99%, the PL spectra peaks are at 484, 457, 458 and 460 nm for *p*TPE-2*m*TPA, *m*TPE-2*o*TPA, *m*TPE-2*m*TPA and *m*TPE-2*p*TPA, respectively, which are all blue-shifted relative to those observed in aqueous mixtures with f_w of 70% (500, 462, 493 and 484 nm, respectively). This should be ascribed to the morphological change of the aggregates from amorphous to crystalline state.[8] That is to say, the molecules are more easily crystallized when the water fraction is increased. From pure THF solution to a THF/H$_2$O mixture containing 95% water, the emission intensities are increased over 300-fold, which can also be verified by visual observations. When illuminated under 365 nm UV lamp, thei THF solutions emitted no observable light, but intense emissions were clearly observed from the THF/H$_2$O mixture with 95% water content (Fig. 3A).
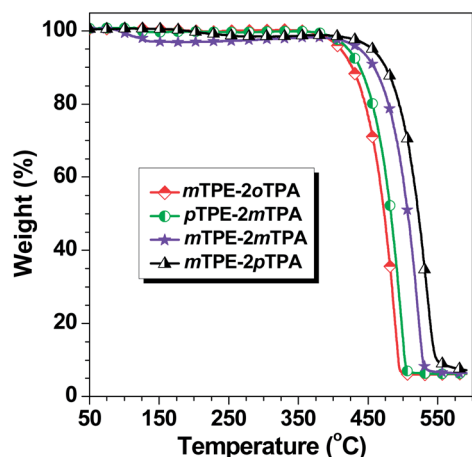

Fig. 1 TGA curves of Methyl-**BTPE**, Isopro-**BTPE**, Ph-**BTPE** and Cz-**BTPE** recorded under N$_2$ at a heating rate of 10 °C min.

2030 | *J. Mater. Chem. C*, 2014, **2**, 2028–2036

This journal is © The Royal Society of Chemistry 2014

Table 1 The thermal, electrochemical and photophysical data of the TPE-based luminogens

	$T_d{}^a$ °C	$Tg{}^b$ °C	$E_g{}^c$ eV	$E_{HOMO}{}^d$ eV	$E_{LUMO}{}^e$ eV	PL λ_{max} Aggr^f nm	Film nm	Φ_F (%) Aggr^f	λ_{abs} Soln^g nm
*p*TPE-2*m*TPA	422	—	3.21	−5.25	−2.04	484	483	64.4	350, 300
*m*TPE-2*o*TPA	411	—	3.36	−5.27	−1.91	457	458	40.4	300
*m*TPE-2*m*TPA	438	82	3.45	−5.25	−1.80	458	459	47.8	299
*m*TPE-2*p*TPA	457	87	3.33	−5.19	−1.86	460	461	35.2	327

^{a} 5% weight loss temperature measured by TGA under N_2. ^{b} Glass-transition temperature measured by DSC under N_2. ^{c} Band gap estimated from optical absorption band edge of the solution. ^{d} Calculated from the onset oxidation potentials of the compounds. ^{e} Estimated using empirical equations $E_{LUMO} = E_{HOMO} + E_g$. ^{f} Determined in THF : H_2O = 1 : 99 solution. ^{g} Observed from absorption spectra in dilute THF solution, 10 μM.
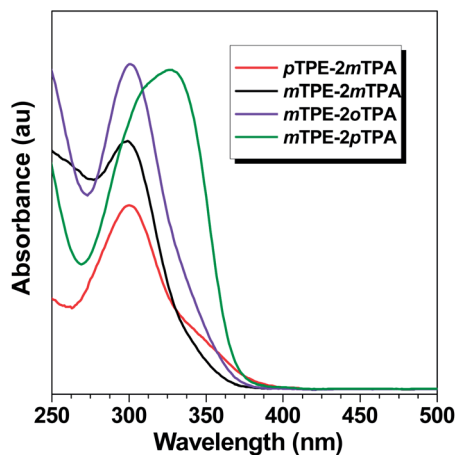

Fig. 2 UV spectra of *p*TPE-2*m*TPA, *m*TPE-2*o*TPA, *m*TPE-2*m*TPA and *m*TPE-2*p*TPA in THF solution. Concentration (μM): ∼10.

Among them, *p*TPE-2*m*TPA in the mixed solvent emits almost green light, which is significantly red-shifted in comparison to the other analogues, indicating its better conjugated structure. However, when more water is added (f_w = 99%), the emissions of the four fluorophores in the aqueous mixtures decreased to some extent, probably due to their relative poor solubility
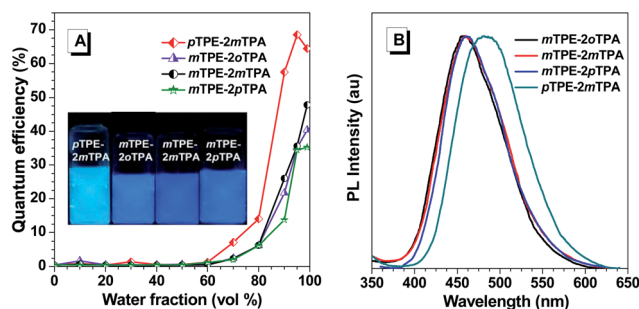

Fig. 3 (A) Plots of fluorescence quantum yields of *p*TPE-2*m*TPA, *m*TPE-2*o*TPA, *m*TPE-2*m*TPA and *m*TPE-2*p*TPA determined in THF/ H_2O solutions using 9,10-diphenylanthracene (Φ = 90% in cyclohexane) as standard *versus* water fractions. Inset: photos of the luminogens in THF/water mixture (f_w = 99%) taken under the illumination of a 365 nm UV lamp; (B) the PL spectra of the films of the four compounds. The thin films were spin-coated onto ITO glass from dilute THF solution with concentrations of ∼1 mg mL^{-1}.

caused by their rigid molecular structures. The quantitative enhancement of emission was evaluated by the PL quantum yields (Φ_F), using 9,10-diphenylanthracene as the standard. From pure solution in THF to the aggregated state in a 99% aqueous mixture, the Φ_F values of *p*TPE-2*m*TPA increased from 0.5% to 64.4%. Similar phenomena were also observed for the other three luminogens. The quantum yields were up to 40.4%, 47.8% and 35.2%, for *m*TPE-2*o*TPA, *m*TPE-2*m*TPA and *m*TPE-2*p*TPA in 99% aqueous mixture, respectively. Evidently, these four **2TPATPE** derivatives are all AIE-active.

Furthermore, we have also investigated the PL properties of the four fluorophores in the solid state, as luminescent materials are often fabricated as thin solid films for their practical applications. As shown in Fig. 3B, for *m*TPE-2*o*TPA, *m*TPE-2*m*TPA and *m*TPE-2*p*TPA, they all exhibit blue emissions in the range of 458–461 nm, which are similar values to those observed in aqueous mixtures. However, the solid emission of *p*TPE-2*m*TPA is significantly red-shifted with a PL peak at 483 nm, in the sky-blue region. This is in consistent with the visual observations of the four compounds under identical conditions, indicating the more conjugated molecular structure of *p*TPE-2*m*TPA than those of the other three molecules.

Electrochemical properties

Cyclic voltammetry (CV) was carried out to investigate the electrochemical properties of the four **2TPATPE** derivatives. The highest occupied molecular orbital (HOMO) energy levels were estimated from the onset oxidation potentials according to the equation: HOMO = −(4.8 + E_{ox}) eV, while the lowest unoccupied molecular orbital (LUMO) energy levels were obtained from optical band-gap energies (estimated from the onset wavelengths of the UV absorptions) and HOMO values. For *p*TPE-2*m*TPA, *m*TPE-2*o*TPA, *m*TPE-2*m*TPA and *m*TPE-2*p*TPA (Fig. S3†), their HOMO values are calculated to be −5.25, −5.27, −5.25 and −5.19 eV, respectively, which are very close to that of *N*,*N*′-bis-(naphthalen-1-y)-*N*,*N*′-bis(phenyl)benzidine (NPB, −5.30 eV). The small energy gap between the hole-transporting layer (NPB) and emissive layers suggests efficient charge transfer in the OLEDs, thus a low turn-on voltage and high luminescence of the device. Moreover, the smaller band-gap energy of *p*TPE-2*m*TPA (3.21 eV) has demonstrated its longer effective conjugation, which will lead to a more red-shifted EL emission. However, all of the four derivatives possess much larger band gaps than that of **2TPATPE**

This journal is © The Royal Society of Chemistry 2014

J. Mater. Chem. C, 2014, **2**, 2028–2036 | **2031**

(1.8 eV), further proving the powerful structural adjustment for controllable emissions by simply changing the linkage modes. As a result, the EL emissions of the new luminogens should be largely blue-shifted. Accordingly, their LUMO energy levels are calculated to be −2.04, −1.91, −1.80 and −1.86 eV, respectively.

Theoretical calculations

To further understand the structure–property relationship at the molecular level, Density Functional Theory (DFT) calculations (B3LYP/6-31g*) of the four luminogens were carried out to obtain the optimized structures and orbital distributions of HOMO and LUMO energy levels of *p*TPE-2*m*TPA, *m*TPE-2*o*TPA, *m*TPE-2*m*TPA and *m*TPE-2*p*TPA, respectively. As demonstrated in Fig. 4, the electron clouds of HOMO energy levels are all mainly located on the **TPA** moieties, due to the good electron-donating and hole-transporting abilities of **TPA**, while the LUMOs of the four chromophores are dominated by orbitals from the **TPE** core. Such electron distributions disclose their weak intramolecular charge transfer property, which will lead to their controllable blue or almost deep-blue emissions. As reported in the literature, **2TPATPE** is a mixture of *E*- and *Z*-isomers. For *E*-**2TPATPE**, its molecular orbitals are more delocalized, explaining its much higher intramolecular conjugation and redder emission than these four derivatives with certain *Z*-configurations presented in this paper. This is in good accordance with the optical properties discussed above and theoretically fulfils our design idea of generating blue AIE emitters by changing the linking positions. Moreover, for *m*TPE-2*o*TPA, the dihedral angle between the adjacent phenyl blades of **TPE** and **TPA** is ∼52°, much higher than those of **2TPATPE** and the other three chromophores (∼36°). It shows that *m*TPE-2*o*TPA possesses the most twisted conformation among the four **2TPATPE** derivatives, which can also be easily seen from their optimized structures (Fig. 5).

Electroluminescence

The good thermal stability and efficient solid-state emission of these materials prompt us to investigate their electroluminescence properties. We have fabricated non-doped devices with a configuration of ITO/MoO₃ (10 nm)/NPB (60 nm)/EML (15 nm)/TPBi (35 nm)/LiF (1 nm)/Al (100 nm) under identical conditions. In these OLED devices, MoO₃, NPB, and TPBi worked as the hole-injection, hole-transporting, and hole-blocking layers respectively, and *p*TPE-2*m*TPA, *m*TPE-2*o*TPA, *m*TPE-2*m*TPA and *m*TPE-2*p*TPA served as emitters. Fig. 6 shows the current density–voltage–brightness (*J–V–L*) characteristics, current efficiency *versus* current density curves and EL spectra of the OLEDs, and the EL data are listed in Table 2. The device based on *m*TPE-2*p*TPA exhibited the lowest turn-on voltage of 2.4 V owing to its higher HOMO energy level, compared to those of *p*TPE-2*m*TPA, *m*TPE-2*o*TPA and *m*TPE-2*m*TPA (4.0, 4.0 and 5.0 V, respectively). As shown in the current density–voltage–luminance (*J–V–L*) curves (Fig. 6a), the current densities increase rapidly with increasing voltage. Better EL performance was observed for *p*TPE-2*m*TPA with L_{max}, $\eta_{C,max}$, and $\eta_{P,max}$ of 8160 cd m⁻², 3.79 cd A⁻¹, and 2.94 lm W⁻¹ respectively. *p*TPE-2*m*TPA, has a smaller band gap (3.21 eV) and lower LUMO energy level (−2.04 eV) than those of the other three molecules (3.36 to 3.45 eV, −1.91 to −1.80 eV), which is beneficial for the charge injection from the adjacent layers (NPB and TPBi) to the emissive layer. As a result, *p*TPE-2*m*TPA shows a higher device performance. As we have reported previously,[10] there is a balance between good electroluminescence performance and controllable EL emission. Although the EL data are not as good as those of **2TPATPE**, to our surprise, the EL emission of *p*TPE-2*m*TPA is dramatically blue-shifted from 514 to 466 nm, with CIE coordinates of (0.17, 0.22) in the sky-blue region. More importantly, *p*TPE-2*m*TPA was conveniently synthesized with confirmed chemical structure, and without a mixture of *E*- and *Z*-isomers as is the case for **2TPATPE**, and the two **TPA** units were linked to the **TPE** core through their *meta*-positions. Thus, this successful attempt indeed verifies the effectiveness of the minor structural modification of changing linking positions.

With the purpose of constructing deep-blue AIE luminogens, a **TPE** core with *m*, *m*-linkage modes has also subsequently been
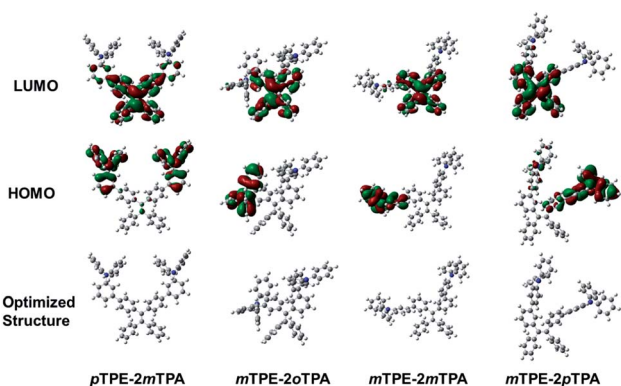

Fig. 4 Calculated molecular orbital amplitude plots of HOMO and LUMO levels and optimized molecular structures of *p*TPE-2*m*TPA, *m*TPE-2*o*TPA, *m*TPE-2*m*TPA and *m*TPE-2*p*TPA.
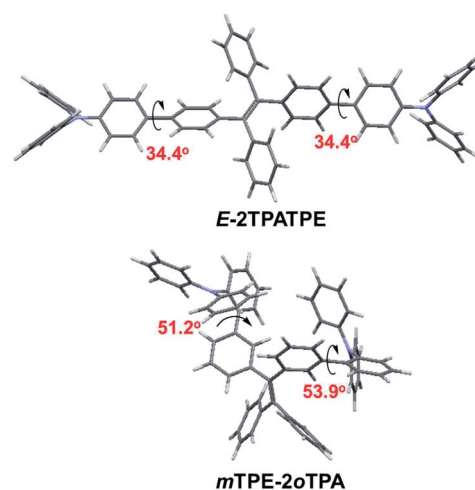

Fig. 5 The dihedral angles of the phenyl blades between **TPE** and **TPA** moieties according to the optimized structures of *E*-**2TPATPE** and *m*TPE-2*o*TPA.

2032 | *J. Mater. Chem. C*, 2014, **2**, 2028–2036

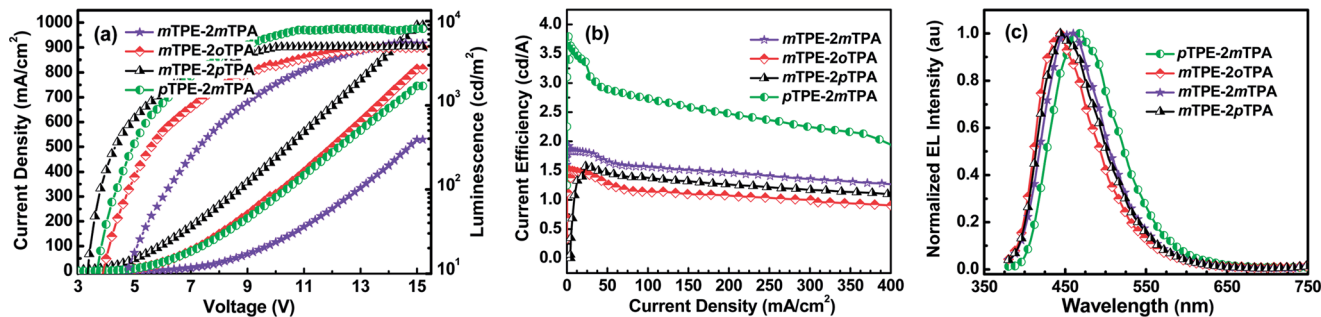This journal is © The Royal Society of Chemistry 2014

Fig. 6 (a) Current density–voltage–luminance characteristics of multilayer EL devices of *p*TPE-2*m*TPA, *m*TPE-2*o*TPA, *m*TPE-2*m*TPA and *m*TPE-2*p*TPA. (b) Change in current efficiency with the current density in multilayer EL devices. (c) EL spectra of the luminogens. Device configurations: ITO/NPB(60 nm)/EML(20 nm)/TPBi(40 nm)/LiF (1 nm)/Al.

Table 2 EL performances of the **TPE**-based luminogens[a]

	λ_{EL} (nm)	V_{on} (V)	L_{max} (cd m^{-2})	$\eta_{C,max}$ (cd A^{-1})	$\eta_{P,max}$ (Im W^{-1})	CIE (x,y)
*p***TPE**-2*m***TPA**	466	4.0	8160	3.79	2.94	0.17, 0.22
*m***TPE**-2*o***TPA**	443	4.0	4880	1.51	1.15	0.16, 0.13
*m***TPE**-2*m***TPA**	454	5.0	5480	1.92	1.49	0.16, 0.16
*m***TPE**-2*p***TPA**	445	2.4	5020	1.57	1.12	0.16, 0.15

[a] Abbreviations: V_{on} = turn-on voltage at 1 cd m^{-2}, L_{max} = maximum luminance, $\eta_{P,max}$ and $\eta_{C,max}$ = maximum power and current efficiencies, respectively. CIE = Commission International de l'Eclairage coordinates.

utilized. As expected, devices based on the other three emitters, *m***TPE**-2*o***TPA**, *m***TPE**-2*m***TPA** and *m***TPE**-2*p***TPA**, all exhibit almost deep-blue emissions ranging from 443–454 nm with CIE coordinates of (0.16, 0.13), (0.16, 0.16) and (0.16, 0.15), respectively. Among them, *m***TPE**-2*m***TPA** possesses the best EL performance with L_{max}, $\eta_{C,max}$, and $\eta_{P,max}$ of 5480 cd m^{-2}, 1.92 cd A^{-1}, and 1.49 Im W^{-1}, compared to *m***TPE**-2*o***TPA** and *m***TPE**-2*p***TPA** with L_{max}, $\eta_{C,max}$, and $\eta_{P,max}$ of 4880 and 5020 cd m^{-2}, 1.51 and 1.57 cd A^{-1}, and 1.15 and 1.12 Im W^{-1}, respectively. For *p***TPE**-2*m***TPA**, when the linking positions of the **TPE** core are changed from *para* to *meta*, the EL peak of the resultant luminogen *m***TPE**-2*m***TPA** is blue-shifted from 466 (sky-blue) to 454 nm (almost deep-blue), further realizing our idea of generating blue emitters and demonstrating that **TPE** with *m*, *m*-linkage mode should be an effective and promising building block for AIE molecules with limited conjugation.

Compared to **2TPATPE** which exhibits a green emission (514 nm), light-emitting devices based on the four new derivatives exhibit blue or almost deep-blue emissions, confirming the control of light-emission through a very simple strategy with a minor structural modification. The ingenious employment of a **TPE** core with *m*, *m*-linkage mode and *o*-, *m*-, or *p*-**TPA** has greatly decreased the intramolecular conjugation of **2TPATPE**, resulting in their blue EL emissions and good device performance. This is consistent with our previous reports[10c] and also gives some insight into further molecular design. Thus, the above results once again confirmed that in the disubstituted

benzene derivatives, there is nearly no conjugation between the two substituted groups in the *meta*-positions, leading to the shorter conjugation length of the resultant molecule. However, when the two groups are in the *ortho*-positions, although there are some conjugation effects, the highly twisted structure will decrease the conjugation length. Surely, a good conjugation effect with the longest conjugation length will be achieved for the *para*-positions.

As shown in Chart 3, there are four *meta*-positions in a **TPE** unit. The pleasing results obtained by using one and two *meta*-substituted **TPE**, inspire us to expand our blue and deep-blue AIE systems by taking three or all *meta*-substituted **TPE** as building blocks. Thus, in addition to the small blue AIE molecules, linear or hyperbranched polymers could also be conveniently constructed with controllable EL emissions, and the related work is under way in our lab.

Conclusions

In this work, we have successfully synthesized four **2TPATPE** derivatives, namely *p***TPE**-2*m***TPA**, *m***TPE**-2*o***TPA**, *m***TPE**-2*m***TPA** and *m***TPE**-2*p***TPA**, in an effort to generate blue or deep-blue AIE emitters. By employing the **TPE** core with *m*, *m*-linkage mode, the torsion degree between the **TPE** and **TPA** units could be significantly increased, and as a result, the π-conjugation lengths of the four luminogens have been effectively shortened. When fabricated as emissive layers in OLEDs, all of the four emitters exhibit blue to almost deep-blue emissions ranging
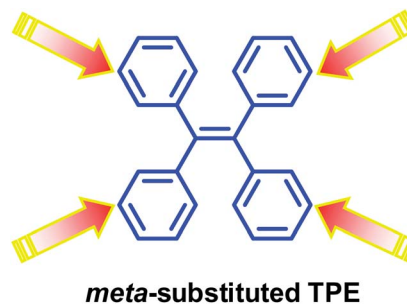

meta-substituted TPE

Chart 3 *Meta*-substituted positions of TPE.

from 443 to 466 nm with L_{max} and $\eta_{C,max}$ up to 8160 cd m^{-2} and 3.79 cd A^{-1}, and CIE coordinates of (0.17, 0.22), (0.16, 0.13), (0.16, 0.16) and (0.16, 0.15) respectively, but not the green emission of **2TPATPE**. In other words, the minor structural modifications have led to significant blue-shifted emissions, which is proven to be an efficient approach to tune the conjugation of the whole luminogens. Considering the previous studies, our further work will focus on the construction of more excellent small blue and deep-blue AIE molecules and polymers with enhanced EL efficiencies, by further application of our idea of utilizing the different linkage mode.

Experimental section

Characterization

^{1}H and ^{13}C NMR spectra were measured on a MECUYRVX300 spectrometer. Elemental analyses of carbon, hydrogen, and nitrogen were performed on a CARLOERBA-1106 microanalyzer. Mass spectra were measured on a ZAB 3F-HF mass spectrophotometer. UV-vis absorption spectra were recorded on a Shimadzu UV-2500 recording spectrophotometer. Photoluminescence spectra were recorded on a Hitachi F-4500 fluorescence spectrophotometer. Differential scanning calorimetry (DSC) was performed on a Mettler Toledo DSC 822e at a heating and cooling rate of 10 °C min^{-1} from room temperature to 250 °C under nitrogen. The glass transition temperature (T_g) was determined from the second heating scan. Thermogravimetric analysis (TGA) was undertaken using a NETZSCH STA 449C instrument. The thermal stability of the samples under a nitrogen atmosphere was determined by measuring their weight loss while heating at a rate of 10 °C min^{-1} from 25 to 600 °C. Cyclic voltammetry (CV) was carried out on a CHI voltammetric analyzer in a three-electrode cell with a Pt counter electrode, an Ag/AgCl reference electrode, and a glassy carbon working electrode at a scan rate of 100 mV s^{-1} with 0.1 M tetrabutylammonium perchlorate (purchased from Aldrich) as the supporting electrolyte, in anhydrous dichloromethane solution purged with nitrogen. The potential values obtained in reference to the Ag/Ag$^+$ electrode were converted to values *versus* the saturated calomel electrode (SCE) by means of an internal ferrocenium/ferrocene (Fc$^+$/Fc) standard.

Computational details

The geometrical and electronic properties were optimized at B3LYP/6-31g(d) level using Gaussian 09 program. The molecular orbitals were obtained at the same level of theory.

OLED device fabrication and measurement

The devices were fabricated on 80 nm ITO-coated glass with a sheet resistance of 25 Ω □$^{-1}$. Prior to loading into the pretreatment chamber, the ITO-coated glass was soaked in ultrasonic detergent for 30 min, followed by spraying with de-ionized water for 10 min, soaking in ultrasonic de-ionized water for 30 min, and oven-baking for 1 h. The cleaned samples were treated by perfluoromethane (CF4) plasma with a power of 100 W, gas flow of 50 sccm, and pressure of 0.2 Torr for 10 s in

the pretreatment chamber. The samples were transferred to the organic chamber with a base pressure of 7 × 10^{-7} Torr for the deposition of *N,N*-bis(1-naphthyl)-*N,N*-diphenylbenzidine (NPB), emitters, 2,2′,2″-(1,3,5-benzinetriyl)tris(1-phenyl-1-*H*-benzimidazole) (TPBi), which served as hole-transporting, light-emitting, hole-blocking, and electron-transporting layers, respectively. The samples were then transferred to the metal chamber for cathode deposition which composed of 1 nm lithium fluoride (LiF) capped with 100 nm aluminum (Al). The light-emitting area was 4 mm^2. The current density–voltage characteristics of the devices were measured by a HP4145B semiconductor parameter analyzer. The forward direction photons emitted from the devices were detected by a calibrated UDT PIN-25D silicon photodiode. The luminance and external quantum efficiencies of the devices were inferred from the photocurrent of the photodiode. The electroluminescence spectra were obtained using a PR650 spectrophotometer. All the measurements were carried out under air at room temperature without device encapsulation.

Preparation of nanoaggregates

Stock THF solutions of the fluorophores were prepared with a concentration of 10^{-3} mol L^{-1}. Aliquots of the stock solution were transferred to 10 mL colorimetric cylinders. Then appropriate amounts of THF and water were added successively under vigorous shaking to furnish 10^{-5} M solutions with different water fractions (0–99.9 vol%). The PL measurements of the resultant solutions were then performed immediately.

Preparation of compounds

All other chemicals and reagents were obtained from commercial sources and used as received without further purification. Solvents for chemical synthesis were purified according to the standard procedures.

Synthesis of compound 1

A solution of 1.3 M *i*PrMgCl·LiCl in THF (4.5 mL) was added dropwise to 1,3-dibromobenzene (1.39 g, 5.9 mmol) in anhydrous THF (20 mL) under N$_2$ at −20 °C. After 0.5 h, the mixture was warmed to room temperature, stirred for 2 h and cooled to −20 °C again. Then, 3-bromobenzaldehyde (0.6 mL, 5 mmol) was added to the mixture at −20 °C. The reaction mixture was stirred for another 2 h at −10 °C and then allowed to reach room temperature overnight. After hydrolysis with saturated NH$_4$Cl solution, the mixture was extracted with CH$_2$Cl$_2$ (3 × 50 mL). The combined organic layers were dried over Na$_2$SO$_4$ and evaporated under reduced pressure. The crude product was used for next step without further purification.

Synthesis of 3,3′-dibromobenzophenone (2)

To a solution of compound **1** (5 mmol) in CH$_2$Cl$_2$ (50 mL), pyridinium chlorochromate complex (1.08 g, 5 mmol) was added with several portions. The reaction mixture was stirred at room temperature for 3 h. After vacuum filtration, the filtrate was evaporated under reduced pressure. The crude product was

purified by flash chromatography using petroleum ether/ethyl acetate as eluent to obtain a white solid in the yields of 52%. ^{1}H NMR (300 MHz, CDCl$_3$) δ (ppm): 7.93 (s, 2H), 7.76–7.68 (m, 4H), 7.41–7.36 (t, 2H).

Synthesis of compound 3

A 2.1 M solution of *n*-butyllithium in hexane (6 mmol, 2.9 mL) was added to a solution of diphenylmethane (1.26 g, 7.5 mmol) in anhydrous tetrahydrofuran (20 mL) at 0 °C under an N$_2$ atmosphere. After stirring for 1 h at this temperature, 4,4′-dibromobenzophenone (1.69 g, 5 mmol) was added. After 2 h, the mixture was slowly warmed to room temperature. Then, the reaction was quenched with an aqueous solution of ammonium chloride and the mixture was extracted with dichloromethane. The organic layer was evaporated after drying with anhydrous sodium sulfate and the resultant crude product was dissolved in toluene (20 mL). The *p*-toluenesulfonic acid (0.17 g, 1 mmol) was added, and the mixture was refluxed overnight and cooled to room temperature. The mixture was evaporated and the crude product was purified by silica gel column chromatography using petroleum ether as eluent to obtain a white powder (3) in the yield of 62%. ^{1}H NMR (300 MHz, CDCl$_3$) δ (ppm): 7.36–7.21 (m, 5H), 7.14–7.12 (m, 6H), 7.01–6.99 (m, 4H), 6.88–6.85 (m, 3H).

Synthesis of compound 4

Prepared by following the similar procedure to compound 3 from 3,3′-dibromobenzophenone (2). White solid. Yield: 65%. ^{1}H NMR (300 MHz, CDCl$_3$) δ (ppm): 7.25–7.23 (m, 2H), 7.14–7.11 (m, 8H), 7.00–6.95 (m, 8H).

Synthesis of compound 5

A mixture of compound 3 (4.90 g, 10 mmol), 4,4,4′,4′,5,5,5′,5′-octamethyl-2,2′-bi(1,3,2-dioxaborolane) (6.35 g, 25 mmol), potassium acetate (6.87 g, 70 mmol), and Pd(dppf)Cl$_2$ (0.15 g, 0.2 mmol) in anhydrous 1,4-dioxane (80 mL) were refluxed under N$_2$ for 12 h, and then water (20 mL) was added. The crude product was extracted into ethyl acetate, washed with water, and dried over anhydrous sodium sulfate. After removing solvent under reduced pressure, the residue was purified by column chromatography using petroleum ether 60–90 °C and ethyl acetate (v/v 10/1) as eluent. A white powder of 5 was obtained in the yield of 68.9% (4.2 g). ^{1}H NMR (300 MHz, CDCl$_3$) δ (ppm): 7.53–7.47 (m, 4H), 7.11–7.09 (m, 4H), 7.07–7.05 (m, 6H), 7.00–6.98 (m, 4H), 1.26 (s, 12H).

Synthesis of compound 6

Prepared by following the similar procedure to compound 5 from 3,3′-dibromotetraphenylethene (4). White solid. Yield: 57%. ^{1}H NMR (300 MHz, CDCl$_3$) δ (ppm): 7.52–7.47 (m, 4H), 7.11–7.10 (m, 14H), 1.27 (s, 12H).

Synthesis of *p*TPE-2*m*TPA

A mixture of compound 5 (520 mg, 0.89 mmol), 3-bromo-triphenylamine (667 mg, 1.80 mmol), Pd(PPh$_3$)$_4$ (30 mg) and potassium hydroxide (560 mg, 10 mmol) in THF (15 mL) and distilled water (5 mL) was refluxed for 2 days under N$_2$ in a 50 mL schlenk tube. The mixture was extracted with dichloromethane. The combined organic extracts were dried over anhydrous Na$_2$SO$_4$ and concentrated by rotary evaporation. The crude product was purified by column chromatography on silica gel using dichloromethane/petroleum ether as eluent to afford the product as white powder in the yield of 75%. ^{1}H NMR (300 MHz, CDCl$_3$) δ (ppm): 7.30–7.24 (m, 21H), 7.11–7.09 (m, 13H), 7.04–7.02 (m, 12H). ^{13}C NMR (100 MHz, CDCl$_3$) δ (ppm): 148.4, 148.0, 143.9, 143.1, 141.9, 141.4, 140.2, 138.7, 132.0, 131.5, 129.7, 129.4, 128.0, 126.7, 126.4, 124.3, 123.4, 123.3, 122.9, 121.6. MS (EI), *m/z*: 818.52 ([M$^+$], calcd for C$_{62}$H$_{46}$N$_2$, 818.37). Anal. calcd for C$_{62}$H$_{46}$N$_2$: C, 90.92; H, 5.66; N, 3.42. Found: C, 90.55; H, 5.75; N, 3.15.

Synthesis of *m*TPE-2*o*TPA

Prepared following the similar procedure to *p*TPE-2*m*TPA from compound 6 and 2-bromotriphenylamine. White solid. Yield: 45%. ^{1}H NMR (300 MHz, CDCl$_3$) δ (ppm): 7.26–7.15 (m, 9H), 7.10–7.03 (m, 13H), 6.90–6.69 (m, 20H), 6.58–6.47 (m, 4H). ^{13}C NMR (100 MHz, CDCl$_3$) δ (ppm): 147.6, 144.6, 144.2, 143.1, 141.1, 141.0, 140.5, 140.4, 140.2, 138.8, 132.3, 131.6, 130.2, 129.6, 129.3, 128.9, 127.8, 126.9, 126.7, 126.5, 126.4, 125.8, 122.2, 121.4. MS (EI), *m/z*: 818.27 ([M$^+$], calcd for C$_{62}$H$_{46}$N$_2$, 818.37). Anal. calcd for C$_{62}$H$_{46}$N$_2$: C, 90.92; H, 5.66; N, 3.42. Found: C, 90.59; H, 5.43; N, 3.12.

Synthesis of *m*TPE-2*m*TPA

Prepared following the similar procedure to *m*TPE-2*m*TPA from compound 6 and 3-bromotriphenylamine. White solid. Yield: 61.1%. ^{1}H NMR (300 MHz, CDCl$_3$) δ (ppm): 7.24–7.22 (m, 18H), 7.15–7.07 (m, 8H), 6.98–6.85 (m, 20H). ^{13}C NMR (100 MHz, CDCl$_3$) δ (ppm): 148.2, 148.0, 143.8, 142.4, 141.9, 140.8, 140.1, 131.3, 130.9, 130.4, 129.6, 129.4, 128.3, 128.0, 126.7, 125.4, 124.1, 123.6, 123.3, 122.8, 122.0. MS (EI), *m/z*: 818.54 ([M$^+$], calcd for C$_{62}$H$_{46}$N$_2$, 818.37). Anal. calcd for C$_{62}$H$_{46}$N$_2$: C, 90.92; H, 5.66; N, 3.42. Found: C, 91.09; H, 5.17; N, 3.04.

Synthesis of *m*TPE-2*p*TPA

Prepared following the similar procedure to *m*TPE-2*p*TPA from compound 6 and 4-bromotriphenylamine. White solid. Yield: 40.1%. ^{1}H NMR (300 MHz, CDCl$_3$) δ (ppm): 7.29–7.22 (m, 11H), 7.18–7.07 (m, 26H), 7.04–6.99 (m, 9H). ^{13}C NMR (100 MHz, CDCl$_3$) δ (ppm): 147.8, 147.1, 144.0, 143.9, 141.6, 141.1, 140.0, 135.3, 131.5, 130.4, 130.0, 129.6, 129.4, 128.3, 128.0, 127.9, 126.7, 125.0, 124.4, 124.2, 123.0. MS (EI), *m/z*: 818.57 ([M$^+$], calcd for C$_{62}$H$_{46}$N$_2$, 818.37). Anal. calcd for C$_{62}$H$_{46}$N$_2$: C, 90.92; H, 5.66; N, 3.42. Found: C, 90.43; H, 5.46; N, 3.33.

Notes and references

1 (a) C. W. Tang and S. A. Vanslyke, *Appl. Phys. Lett.*, 1987, **51**, 913; (b) C. W. Tang, S. A. Van Slyke and C. H. Chen, *J. Appl. Phys.*, 1989, **65**, 3610; (c) M. A. Baldo, M. E. Thompson and S. R. Forrest, *Nature*, 2000, **403**, 750; (d) B. W. D'Andrade and S. R. Forrest, *Adv. Mater.*, 2004, **16**, 1585.

2 (a) T. P. I. Saragi, T. Spehr, A. Siebert, T. Fuhrmann-Lieker and J. Salbeck, *Chem. Rev.*, 2007, **107**, 1011; (b) R. J. Tseng, R. C. Chiechi, F. Wudl and Y. Yang, *Appl. Phys. Lett.*, 2006, **88**, 093512; (c) K. T. Kamtekar, A. P. Monkman and M. R. Bryce, *Adv. Mater.*, 2010, **22**, 572; (d) L. M. Leung, W. Y. Lo, S. K. So, K. M. Lee and W. K. Choi, *J. Am. Chem. Soc.*, 2000, **122**, 5640; (e) Y. Y. Lyu, J. Kwak, O. Kwon, S. H. Lee, D. Kim, C. Lee and K. Char, *Adv. Mater.*, 2008, **20**, 2720.

3 (a) X. Ren, J. Li, R. J. Holmes, P. I. Djurovich, S. R. Forrest and M. E. Thompson, *Chem. Mater.*, 2004, **16**, 4743; (b) M. T. Lee, C. H. Liao, C. H. Tasi and C. H. Chen, *Adv. Mater.*, 2005, **17**, 2493; (c) B. C. Krummacher, V. E. Choong, M. K. Mathsi, S. A. Choulis, F. Jermann, T. Fiedler and M. Zachau, *Appl. Phys. Lett.*, 2006, **88**, 113506; (d) R. C. Chiechi, R. J. Tseng, F. Marchioni, Y. Yang and F. Wudl, *Adv. Mater.*, 2006, **18**, 325.

4 (a) S. W. Thomas III, G. D. Joly and T. M. Swager, *Chem. Rev.*, 2007, **107**, 1339; (b) A. C. Grimsdale, K. L. Chan, R. E. Martin, P. G. Jokisz and A. B. Holmes, *Chem. Rev.*, 2009, **109**, 897.

5 (a) M. T. Lee, H. H. Chen, C. H. Liao, C. H. Tsai and C. H. Chen, *Appl. Phys. Lett.*, 2004, **85**, 3301; (b) P. F. Wang, Z. R. Hong, Z. Y. Xie, S. W. Tong, O. Y. Wong, C. S. Lee, N. B. Wong, L. S. Hung and S. T. Lee, *Chem. Commun.*, 2003, 1664; (c) S. Hecht and J. M. J. Frechet, *Angew. Chem., Int. Ed.*, 2001, **40**, 74; (d) C. Fan, S. Wang, J. W. Hong, G. C. Bazan, K. W. Plaxco and A. J. Heeger, *Proc. Natl. Acad. Sci. U. S. A.*, 2003, **100**, 6297; (e) S.-F. Lim, R. H. Friend, I. D. Rees, J. Li, Y. Ma, K. Robinson, A. B. Holms, E. Hennebicq, D. Beljonne and F. Cacialli, *Adv. Funct. Mater.*, 2005, **15**, 981.

6 J. Luo, Z. Xie, J. W. Y. Lam, L. Cheng, H. Chen, C. Qiu, H. S. Kwok, X. Zhan, Y. Liu, D. Zhu and B. Z. Tang, *Chem. Commun.*, 2001, 1740.

7 (a) J. Chen, B. Xu, X. Ouyang, B. Z. Tang and Y. Cao, *J. Phys. Chem. A*, 2004, **108**, 7522; (b) Z. Li, Y. Dong, B. Mi, Y. Tang, H. Tong, P. Dong, J. W. Y. Lam, Y. Ren, H. H. Y. Sun, K. Wong, P. Gao, I. D. Williams, H. S. Kwok and B. Z. Tang, *J. Phys. Chem. B*, 2005, **109**, 10061; (c) Y. Ren, J. W. Y. Lam, Y. Dong, B. Z. Tang and K. S. Wong, *J. Phys. Chem. B*, 2005, **109**, 1135; (d) Y. Hong, J. W. Y. Lam and B. Z. Tang, *Chem. Commun.*, 2009, 4332; (e) Y. Hong, J. W. Y. Lam and B. Z. Tang, *Chem. Soc. Rev.*, 2011, **40**, 5361.

8 Y. Dong, J. W. Y. Lam, A. Qin, J. Liu, Z. Li and B. Z. Tang, *Appl. Phys. Lett.*, 2007, **91**, 011111.

9 (a) S. K. Kim, Y. Park, I. N. Kang and J. W. Park, *J. Mater. Chem.*, 2007, **17**, 4670; (b) P. Shih, C. Y. Chuang, C. H. Chien, E. W. G. Diau and C. F. Shu, *Adv. Funct. Mater.*, 2007, **17**, 3141; (c) Z. Zhao, S. Chen, X. Shen, F. Mahtab, Y. Yu, P. Lu, J. W. Y. Lam, H. S. Kwok and B. Z. Tang, *Chem. Commun.*, 2010, **46**, 686; (d) Z. Zhao, S. Chen, J. W. Y. Lam, P. Lu, Y. Zhong, K. S. Wong, H. S. Kwok and B. Z. Tang, *Chem. Commun.*, 2010, **46**, 2221; (e) W. Z. Yuan, P. Lu, S. Chen, J. W. Y. Lam, Z. Wang, Y. Liu, H. S. Kwok, Y. Ma and B. Z. Tang, *Adv. Mater.*, 2010, **22**, 2159; (f) Z. Zhao, J. W. Y. Lam, C. Y. K. Chan, S. Chen, J. Liu, P. Lu, M. Rodriguez, J. L. Maldonado, G. Ramos-Ortiz, H. H. Y. Sung, I. D. Williams, H. Su, K. S. Wong, Y. Ma, H. S. Kwok, H. Qiu and B. Z. Tang, *Adv. Mater.*, 2011, **23**, 5430; (g) Y. Liu, S. Chen, J. W. Y. Lam, P. Lu, R. T. K. Kwok, F. Mahtab, H. S. Kwok and B. Z. Tang, *Chem. Mater.*, 2011, **23**, 2536; (h) Z. Zhao, S. Chen, C. Deng, J. W. Y. Lam, C. Y. K. Chan, P. Lu, Z. Wang, B. Hu, X. Chen, P. Lu, H. S. Kwok, Y. Ma, H. Qiu and B. Z. Tang, *J. Mater. Chem.*, 2011, **21**, 10949; (i) Z. Zhao, C. Deng, S. Chen, J. W. Y. Lam, W. Qin, P. Lu, Z. Wang, H. S. Kwok, Y. Ma, H. Qiu and B. Z. Tang, *Chem. Commun.*, 2011, **47**, 8847; (j) W. Z. Yuan, S. Chen, J. W. Y. Lam, C. Deng, P. Lu, H. H.-Y. Sung, I. D. Williams, H. S. Kwok, Y. Zhang and B. Z. Tang, *Chem. Commun.*, 2011, **47**, 11216; (k) Z. Zhao, P. Lu, J. W. Y. Lam, Z. Wang, C. Y. K. Chan, H. H. Y. Sung, I. D. Williams, Y. Ma and B. Z. Tang, *Chem. Sci.*, 2011, **2**, 672; (l) C. Y. K. Chan, Z. Zhao, J. W. Y. Lam, J. Liu, S. Chen, P. Lu, F. Mahtab, X. Chen, H. H. Y. Sung, H. S. Kwok, Y. Ma, I. D. Williams, K. S. Wong and B. Z. Tang, *Adv. Funct. Mater.*, 2012, **22**, 378; (m) Z. Zhao, J. Geng, Z. Chang, S. Chen, C. Deng, T. Jiang, W. Qin, J. W. Y. Lam, H. S. Kwok, H. Qiu, B. Liu and B. Z. Tang, *J. Mater. Chem.*, 2012, **22**, 11018; (n) Z. Chang, Y. Jiang, B. He, J. Chen, Z. Yang, P. Lu, H. S. Kwok, Z. Zhao, H. Qiu and B. Z. Tang, *Chem. Commun.*, 2013, **49**, 594; (o) Z. Zhao, J. W. Y. Lam and B. Z. Tang, *J. Mater. Chem.*, 2012, **22**, 23726; (p) W. Wu, S. Ye, L. Huang, G. Yu, Y. Liu, J. Qin and Z. Li, *Chin. J. Polym. Sci.*, 2013, **31**, 1432.

10 (a) J. Huang, X. Yang, J. Wang, C. Zhong, L. Wang, J. Qin and Z. Li, *J. Mater. Chem.*, 2012, **22**, 2478; (b) J. Huang, N. Sun, J. Yang, R. Tang, Q. Li, D. Ma, J. Qin and Z. Li, *J. Mater. Chem.*, 2012, **22**, 12001; (c) J. Huang, N. Sun, Y. Dong, R. Tang, P. Lu, P. Cai, Q. Li, D. Ma, J. Qin and Z. Li, *Adv. Funct. Mater.*, 2013, **23**, 2329.

11 S. Bernhardt, M. Baumgarten and K. Müllen, *Eur. J. Org. Chem.*, 2006, 2523.

12 S. Wang, W. J. Oldham, R. A. Hudack and G. C. Bazan, *J. Am. Chem. Soc.*, 2000, **122**, 5695.

13 (a) Y. Tao, Q. Wang, L. Ao, C. Zhong, C. Yang, J. Qin and D. Ma, *J. Phys. Chem. C*, 2010, **114**, 601; (b) S.-J. Su, H. Sasabe, T. Takeda and J. Kido, *Chem. Mater.*, 2008, **20**, 1691.